Intelligent Primary Control of Voltage Source Converters in AC Microgrids

Derbas, Abd Alelah ; Oshnoei, Arman; Kheradmandi, Morteza; Blaabjerg, Frede

Published in:
IECON 2022 – 48th Annual Conference of the IEEE Industrial Electronics Society

Publication date:
2022

Intelligent Primary Control of Voltage Source Converters in AC Microgrids

1st Abd Alelah Derbas
Faculty of Electrical Engineering
Shahid Beheshti University
Tehran, Iran
a_derbas@sbu.ac.ir

2nd Arman Oshnoei
Department of Energy
Aalborg University
9220 Aalborg, Denmark
aros@energy.aau.dk

3rd Morteza Kheradmandi
Faculty of Electrical Engineering
Shahid Beheshti University)
Tehran, Iran
kheradmandi@sbu.ac.ir

4th Frede Blaabjerg
Department of Energy
Aalborg University
9220 Aalborg, Denmark
fbl@energy.aau.dk

IECON 2022 – 48th Annual Conference of the IEEE Industrial Electronics Society | 978-1-6654-8025-3/22/$31.00 ©2022 IEEE | DOI: 10.1109/IECON49645.2022.9969021

***Abstract*—This paper proposes an intelligent primary control strategy for voltage source converter (VSC)-based ac microgrid (MG). This is implemented by using a proportional resonant (PR) regulator adopted in the inner level of primary control of VSCs. An approach based on brain emotional learning (BEL) is proposed to provide an online and adaptive tuning of control coefficients of the PR regulator. The proposed BEL approach is fully model-free, indicating that the coefficients are regulated without previous knowledge of the system model and parameters. The outer level of primary control employs a droop control loop to regulate power-sharing among different distributed generators. Unlike the conventional control methods with constant coefficients, which are typically designed for a specified operating condition, the proposed approach avoids the dependency of the converter control system on the operating conditions and accommodates varying loading conditions. A sensitivity analysis is also performed to investigate the effects of PR coefficients on the system stability. Moreover, a Mesh analysis is carried out to examine the stability of dominant frequency modes of the whole AC-MG using the proposed control scheme. Simulations are provided to demonstrate the performance of the proposed control scheme.**

***Index Terms*—Droop control, proportional resonant control, voltage source converter, brain emotional learning, frequency modes, AC microgrid.**

I. Introduction

Islanded microgrids (MGs) are a group of interconnected loads and distributed generations (DGs) which are connected to the grid through power converters to reduce pollution and power transmission losses and also to obtain high-energy utilization rates with the flexibility of different installation locations. This is an essential concept for future distribution systems and will be more and more used in renewable energy integration, which is the fastest-growing energy source globally [1], [2]. The MGs have higher degrees of controllability in comparison to the conventional generators and can be operated in both grid-connected and islanded-operation modes. Microgrids can be categorized as the Alternating-current (ac) and direct current (dc) MGs. Although dc MGs offer more attractive properties from the viewpoint of performance and control simplicity, most traditional loads demand ac power supply. Hence, it is ordinarily required to implement an ac MG structure after the overall energy conversion chain. Flexible interlinked voltage source converters (VSCs) enable such a structure along with its control functionalities. VSCs operate as interfaces between the flexible loads, the MG's dc and ac parts, and the overhead power grid [3], [4]. To ensure the control of MG dynamics, a hierarchical control structure including primary control (PC), secondary control (SC), and tertiary control (TC) is defined [5]-[7]. The PC stabilizes the voltage and frequency and offers powersharing capability among DGs. The SC can restore the voltage and frequency deviations created by PC operations. The TC handles the power flow management between the grid and MGs at the Point of Common Coupling (PCC). In the PC layer, the reactive power-voltage amplitude and real power-frequency droop control method has been implemented to ensure the advantages of being communicationfree for the power-sharing mechanism, and voltage and frequency stability [8], [9].

Various methods are used to control the interfacing converter of DGs to ensure the satisfactory dynamic performance of MG. The conventional proportional-integral (PI) controllers are the most common techniques in various applications. These controllers, however, may exhibit poor performance with unbalanced current or voltage and harmonics [10]. Proportional resonant (PR) controllers are used extensively due to the ability to eliminate the steady-state error of sinusoidal signal. The low-order harmonic compensation and simple implementation have drawn attention to PR controller as a suitable controller for MGs. The performance of PR controller is mightily influenced by the coefficient values, which are still a challenge to undertake. In this regard, in [11] and [12], the closed-loop poles of the PR regulator are obtained to determine the coefficients. This method, however, demands many computations to cover all the assortments of the possible coefficients. Also, the authors in [13] have used a particle swarm optimization method to determine the coefficients of PR controller. The conducted study for identifying the optimal values of coefficients is, however, dependent on operating conditions, which may give rise to a flawed performance of the MG control system.

Motivated by the above discussion, this paper proposes a model-free and adaptive approach based on brain emotional learning (BEL) to adjust the PR controller coefficients. The proposed BEL-based PR controller is applied to control the VSCs in an islanded ac MG. In this way, neither the parameters nor structures of the system are needed beforehand. The

method offers superior performance in varying operating point conditions. To achieve optimal results with the BEL method working based on the knowledge of the experts, considering favorable scaling factors are the necessary parts, which is also addressed in this paper. In addition, a stability analysis is carried out to examine the stability of the closed-loop control of interfacing converter with the proposed control scheme. Simulations validate the proposed control strategy.

II. Proposed Control Strategy

The single-line diagram of a multi-bus AC-MG, containing three VSC-based DGs is shown in Fig. 1. The AC-MG is assumed to operate in islanded mode. For each DG, the converter model is a two-level three-phase VSC with eight switching states in total. Fig. 2 shows the diagram of a VSC-based DG equipped with the proposed primary control loop. As the figure indicates, a three-phase LC filter is connected to a load to eliminate the harmonics of the output voltage and current. R_f, C_f and L_f are resistance, capacitance and inductance of the LC filter, respectively. The output current (i_o), the filter current (i_f), and output voltage (v_c) are presented in vectors as follows:

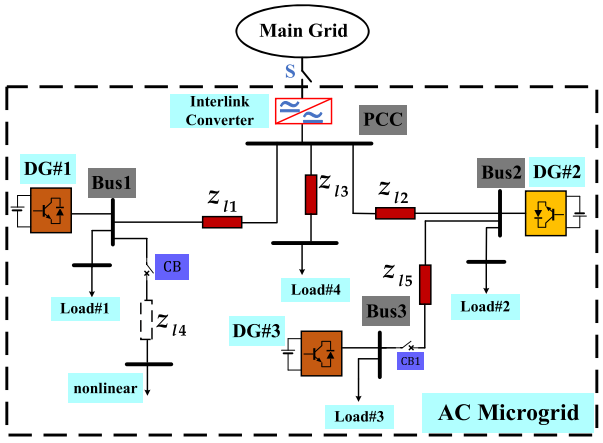

Fig. 1. The single-line diagram of the understudied AC-MG

$$i_o = [i_{ou}, i_{ov}, i_{ow}]^T,\ i_f = [i_{fu}, i_{fv}, i_{fw}]^T,\ v_o = [v_{cu}, v_{cv}, v_{cw}]^T \quad (1)$$

Three-phase variable vectors are transferred to a two-dimensional vector by employing the Clarke transformation (T) as follows:

$$T = 1/3[1, e^{(j2/3\pi)}, e^{(j4/3\pi)}] \quad (2)$$

Finally, the output voltage and current of the converter can be described in the state-space form as follows:

$$\frac{d}{dt}\begin{bmatrix} i_f \\ v_c \end{bmatrix} = \mathbf{A}\begin{bmatrix} i_f \\ v_c \end{bmatrix} + \mathbf{B}\begin{bmatrix} v_i \\ i_0 \end{bmatrix} \quad (3)$$

$$\mathbf{A} = \begin{bmatrix} \frac{R_f}{L_f} & -\frac{1}{L_f} \\ \frac{1}{C_f} & 0 \end{bmatrix}, \quad \mathbf{B} = \begin{bmatrix} \frac{1}{L_f} & 0 \\ 0 & -\frac{1}{C_f} \end{bmatrix} \quad (4)$$

where A and B denote the system and control matrices, respectively, and v_i represents the input voltage. The primary control loop includes a voltage control loop and a droop control loop. The droop control is employed to control active and reactive power-sharing and synchronize each converter. The droop control mechanism can be expressed as

$$f_i = f_0 - m(P_i - P_0) \quad V_{ci} = V_0 - n(Q_i - Q_0) \quad (5)$$

where f_i and V_{ci} are the reference frequency and voltage amplitude, respectively; f_0 and V_0 are the rated of frequency and voltage amplitude, respectively; and m and n are the droop coefficients, which are chosen based on the rated power of the DG unit and the permissible deviations in frequency and voltage amplitude; P_0 and Q_0 are the nominal of active and reactive powers, respectively; and P_i and Q_i are the generated active power and reactive power of DG_i, as follows:

$$P_i = G_L p_i \qquad p_i = V_{c\alpha i} i_{o\alpha i} + V_{c\beta i} i_{o\beta i} \quad (6)$$

$$Q_i = G_L q_i \qquad q_i = V_{c\beta i} i_{o\alpha i} + V_{c\alpha i} i_{o\beta i} \quad (7)$$

where $G_L = \frac{\omega c}{\omega c + s}$ denotes a low-pass filter with cutoff frequency ωc; p_i and q_i are the measured active and reactive powers of DG_i; and v_o and i_o are the instantaneous output voltage and current of DG_i in $\alpha-\beta$ frame. The voltage control loop is composed of an inner loop and an outer loop. The inner current loop is a proportional controller K_c, its gain is adjusted to achieve desired damping ratio and overshoot values of the dominant poles of the current loop.The outer loop uses a PR regulator to avoid the influence of load dynamics and to ensure effective reference tracking caused by the sinusoidal nature of the reference signals. The transfer function of PR regulator can be expressed as follows:

$$G_{PR}(s) = \left(K_P + \frac{K_i s}{s^2 + 2\omega_c s + \omega_o^2}\right) + \Sigma_{h=2n+1}^{\infty} \frac{K_h s}{s^2 + 2h\omega_c s + \omega_h^2}; \quad n = 1, 2, 3, ...\infty \quad (8)$$

where K_P, K_i, and K_h are the proportional gain, the integral gain, and the integral harmonic gain, respectively; w_c is chosen equal to 2 rad/sec. The first part in (8) provides tracking for the first order harmonic of the reference signal with a frequency w_c. The second part represents the harmonics compensator to ensure tracking in case the reference signal includes harmonics. In this paper, a BEL-based method is used so that the PR coefficients are adaptively adjusted. The design procedure of the BEL-based regulation scheme is addressed in the following section.

III. BEL-based Regulation Scheme

The BEL is utilized as a model-free controller in various control engineering applications. The BEL can learn quick-auto, and thus it is proper for robust and fast decision-making in nonlinear systems, especially in systems with uncertainty. In [14], the BEL controller has superior performance compared with PI and fuzzy logic controllers in both online and offline simulations for PMSM drive systems in different test conditions. This method is constituted of Amygdala (AD), which

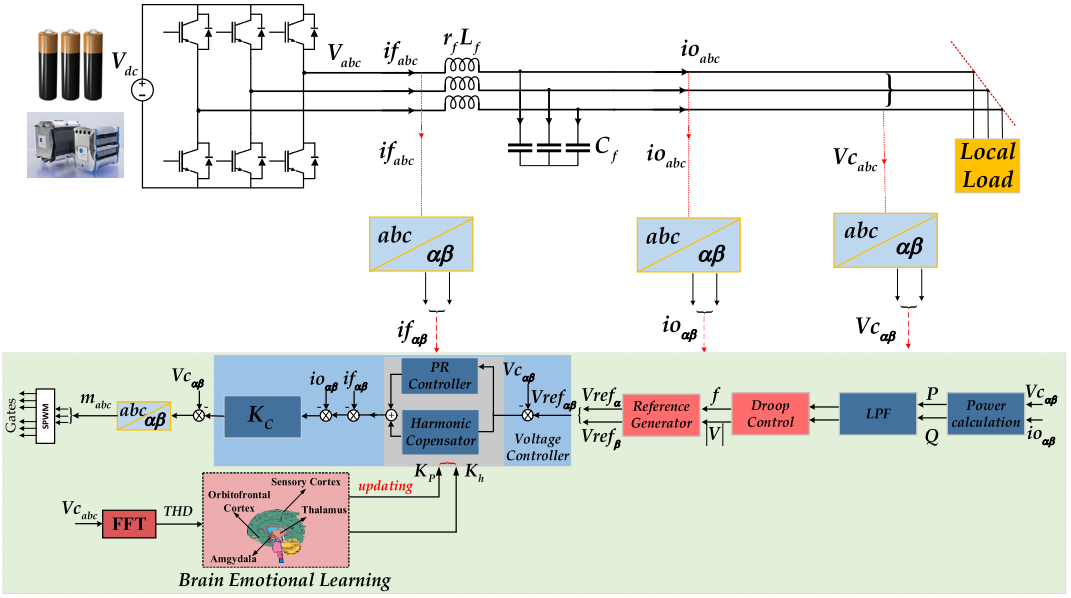

Fig. 2. The block-diagram of the proposed control

is in charge of emotional learning; Orbitofrontal cortex (OC), sensory cortex, and Thalamus [15]. The model is provided with two inputs including sensory input (S) and emotional signal (ES). Preprocessing on SI signal such as filtering or noise reduction is performed by the Thalamus. The sensory cortex receives the Thalamus output and then submits it to the AD and OC. The BEL output is obtained based on the subtraction of outputs of AD and OC networks as follows:

$$M = \sum_{z} A_z - \sum_{z} O_z \tag{9}$$

where A and O denote the functional blocks associated with the AD and OC networks, respectively. The output of AD network is computed as:

$$A_{th} = max(S_z) \tag{10}$$

$$A_z = S_z G_z \tag{11}$$

where A_th is a neuron that receives maximum sensory signals from the thalamus directly.

Similarly, the output of OC network is given by:

$$O_z = S_z H_z \tag{12}$$

The weights in AD and OC networks are updated by using (13) and (14):

$$\Delta G_z = \alpha[S_z max(0, ES - \sum_{z} A_z)] \tag{13}$$

$$\Delta H_z = \gamma[S_z(\sum_{z} O_z - ES)] \tag{14}$$

where α and γ are BEL's learning rates. The schematic diagram of the proposed BEL-based regulation scheme is depicted in Fig. 3. The critical functionality of this structure is to minimize the voltage and frequency variation. The BEL output is supplementary regulation gains to update the constant gains of the PR regulator adaptively. This adaptive feature improves the converter's robustness against different uncertainties and a vast range of working states. To achieve the desired performance of BEL strategy, S and ES are selected as follows:

$$ES = \left(\frac{V_{C_\alpha}^2 + V_{C_\beta}^2}{V_{ref_\alpha}^2}\right) - 1; \qquad S = \left(\frac{f}{f_{ref}}\right) - 1 \tag{15}$$

Two scaling coefficients S_1 and S_2 are considered as the outputs of the intelligent approach. S_1 and S_2 are optimized by a particle swarm optimization algorithm.

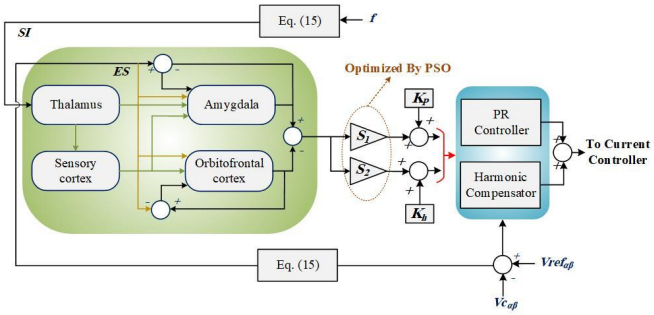

Fig. 3. Schematic of the proposed BEL-based regulation scheme

Remark I. The characteristics of this approach and the major reasons for its choice are twice. First, this approach can generate dynamic outputs for control objectives. This includes producing the control signals in the primary loop concerning the operating point deviations and the event of any disturbance as opposed to the conventional methods.

Second, this intelligent approach has model-free structures whose functionalities are independent of the dynamic model and intricacies of the AC-MG.

IV. Stability Analysis

A. Closed-Loop Control System of VSC

The output voltage of the closed-loop control system can be written as:

$$V_{c_{\alpha\beta}}(s) = H(s)V_{ref_{\alpha\beta}}(s) - Z_{out}(s)i_{o_{\alpha\beta}}(s) \qquad (16)$$

where $Z_{ou}(s)$ is the output impedance of VSC, and $H(s)$ is the transfer fuction of closed-loop system that is calculated by dividing $V_{ref_{\alpha\beta}}(s)$ by $V_{c_{\alpha\beta}}(s)$ as follows:

$$Z_{out}(s) = -\frac{V_{c_{\alpha\beta}}(s)}{i_{o_{\alpha\beta}}(s)}|_{V_{ref_{\alpha\beta}}(s)=0} \quad H(s) = \frac{V_{ref_{\alpha\beta}}(s)}{V_{c_{\alpha\beta}}(s)}|_{i_{o_{\alpha\beta}}(s)=0} \qquad (17)$$

To extract the characteristic equation of the closed-loop control system, the VSC is modeled by an independent voltage source in series with an output impedance. The rest part of AC-MG is represented by a Thevenin voltage source v_{th} together with a Thevenin impedance z_{th}. Then, the characteristic equation is written as follows:

$$Z_{out}(s) \times \Big(R_L + (r_{th} + sl_{th})\Big) + R_L(r_{th} + sl_{th}) = 0. \quad (18)$$

As (18) indicates, the roots of the characteristics equation are impacted by the VSC system parameters. A sensitivity analysis is addressed in the following subsection to examine the effects of the system parameters on the DG stability.

B. Sensitivity Analysis

Here, an eigenvalue analysis is performed to investigate the dynamic performance under varying coefficients of $G_{PR}(s)$. It is presumed that the DGs are in stand-alone operation mode and linked to a local load of $0.05p.u$ through a line, represented with resistance r_l and inductance l_l. At first, to examine the effect of K_P, it is supposed that the coefficients K_I and K_h are equal to zero. Fig. 4 shows the loci of the dominant frequency modes of VSC when K_P value varies from 0.01 to 0. As shown in Fig. 4-(a), the high-frequency modes are little impacted by the K_P gain . The variation of the dominant low-frequency modes of VSC is shown in Fig. 4-(b). As depicted, the VSC stability is enhanced with an increased value of K_P. Now, to analyze the effect of K_I on the stability, it is supposed that both K_P and K_h are set as zero, and the K_I varies from 10 to 500. The variation of the dominant frequency modes of VSC is shown in Fig. 5-(a). As seen, the most impact of coefficient K_I occurs in the medium-frequency modes when K_I changes from 10 to 500. The figure also suggests that the system will be unstable for the K_I values higher than 400. In addition, Fig. 5-(b) shows the dominant frequency modes of VSC for harmonics $h = 3, 5, 7, 9, 11, 13$ when K_h changes from 0.01 to 0.5 (K_I is set as 100). As observed, K_h variations have little effect on the stability region. The frequency response of the open-loop control of VSC is illustrated in Fig. 6. By applying the BEL algorithm, the coefficients K_P, K_I, and K_h are adjusted at 0.11, 100, and 0.2, respectively. Where the desired stability characteristic is achieved, as it is seen, the desired requirements of phase margin and the bandwidth are closed to 60 deg and 1kHz, respectively. In addition, the gain margin of the system at 50Hz and the odd harmonic frequencies are sufficient to eliminate the disturbance. The small-signal model of AC-MG with three DGs is shown in Fig.7, where the linear models of loads, lines, and all DG units are obtained in the Laplace domain. The dominant frequency modes of the overall AC-MG are determined using the characteristic

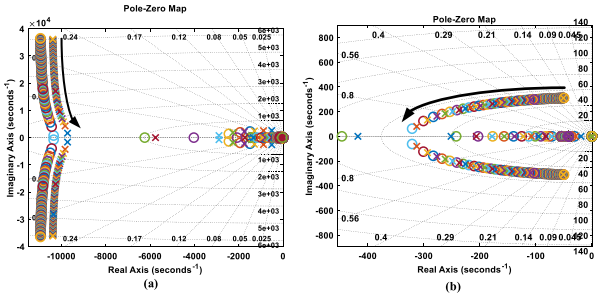

Fig. 4. The dominant frequency modes of VSC when K_P changes from 0.01 to 1, (a) hight-frequency modes, (b) low-frequency modes

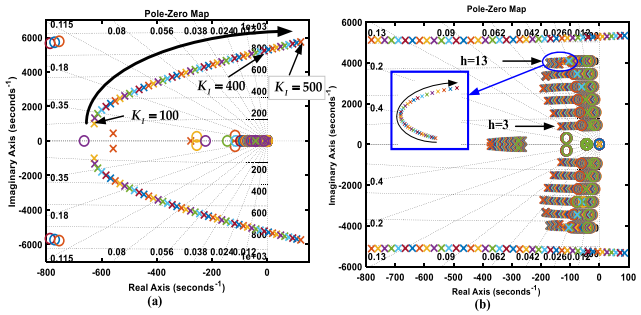

Fig. 5. The dominant frequency modes of VSC, (a) when K_i changes from 10 to 500, (b) when K_h changes from 0.01 to 0.5.

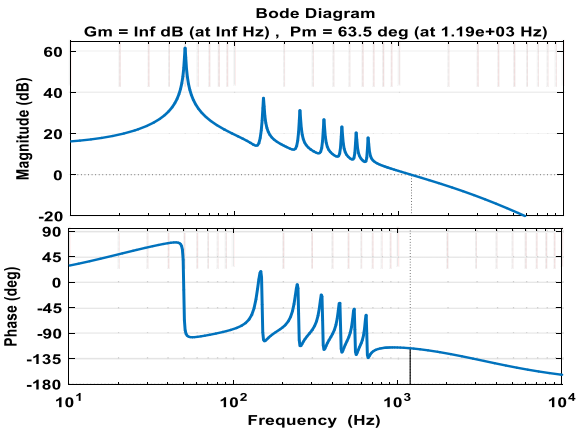

Fig. 6. Frequency response of the open-loop control system

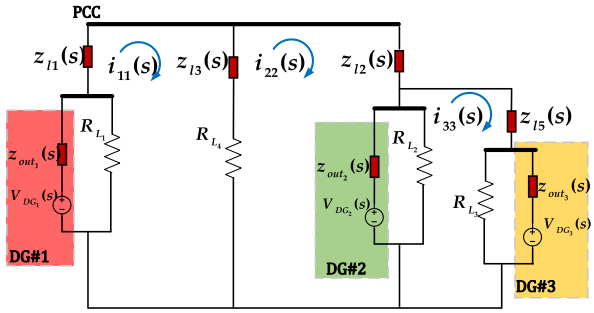

Fig. 7. Equivalent model of overall AC-MG

equation, which is expressed using impedance analysis. The mesh impedance matrix can be calculated as

$$\mathbf{Z_{MG}(s)} = \begin{bmatrix} Z_{\mathrm{MG11}}(s) & Z_{\mathrm{MG12}}(s) & Z_{\mathrm{MG13}}(s) \\ Z_{\mathrm{MG21}}(s) & Z_{\mathrm{MG22}}(s) & Z_{\mathrm{MG23}}(s) \\ Z_{\mathrm{MG31}}(s) & Z_{\mathrm{MG32}}(s) & Z_{\mathrm{MG33}}(s) \end{bmatrix} \tag{19}$$

where

$$\begin{cases} Z_{\mathrm{MG11}}(s) = [Z_{\mathrm{out1}}(s) \parallel R_{\mathrm{L1}} + Z_{L1}(s) + Z_{L3}(s) + R_{\mathrm{L4}}] \\ Z_{\mathrm{MG12}}(s) = Z_{\mathrm{MG21}}(s) = -(Z_{L3}(s) + R_{\mathrm{L4}}) \\ Z_{\mathrm{MG13}}(s) = Z_{\mathrm{MG31}}(s) = 0 \\ Z_{\mathrm{MG22}}(s) = [(Z_{\mathrm{out2}}(s) \parallel R_{\mathrm{L2}} + Z_{L2}(s)) + Z_{L3}(s) + R_{\mathrm{L4}}] \\ Z_{\mathrm{MG23}}(s) = Z_{\mathrm{MG32}}(s) = -(Z_{\mathrm{out2}}(s) \parallel R_{\mathrm{L2}}) \\ Z_{\mathrm{MG33}}(s) = [(Z_{\mathrm{out2}}(s) \parallel R_{\mathrm{L2}}) + (Z_{\mathrm{out3}}(s) \parallel R_{\mathrm{L3}}) \\ +Z_{L5}(s)]. \end{cases} \tag{20}$$

The zero-pole placement of the AC-MG for the designed coefficients of G_{PR} by BEL is displayed in Fig. 8. As the figure demonstrates, a reasonable stability margin has been achieved.

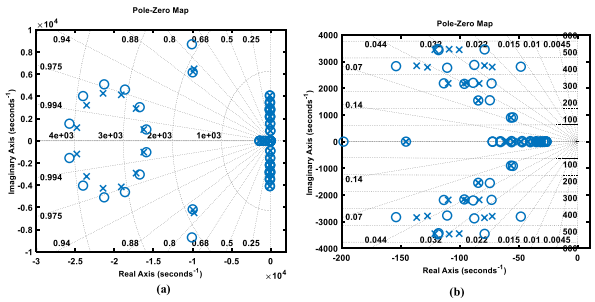

Fig. 8. The dominat frequency mode of AC-MG with three DGs

V. Simulations Results

Various case studies are conducted to assess the performance of the studied AC MG with the proposed control scheme. The AC-MG shown in Fig. 1, including three DGs interfaced with VSC, is simulated in MATLAB/Simulink software environment. The proposed scheme is tested in the following scenarios: (a) Increasing load (a) Imbalance load (a) Nonlinear load, and (a) Plug and play (PnP) operation.

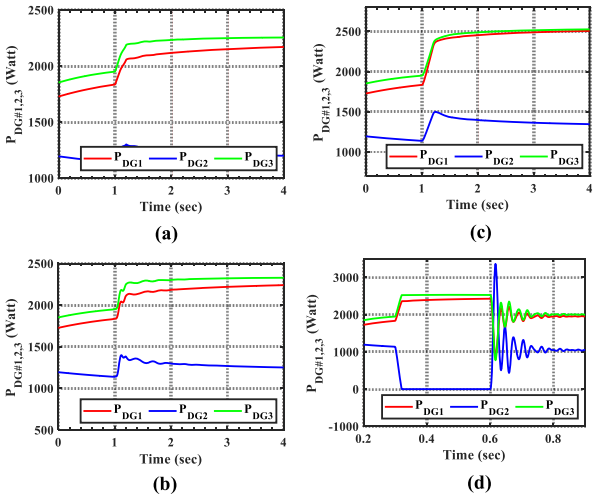

Fig. 9. Dynamic response of AC-MG for various senarios: Active power of DGs (a) increasing load, (b) imbalance load, (c) nonlinear load, (d) plug&play of DG2

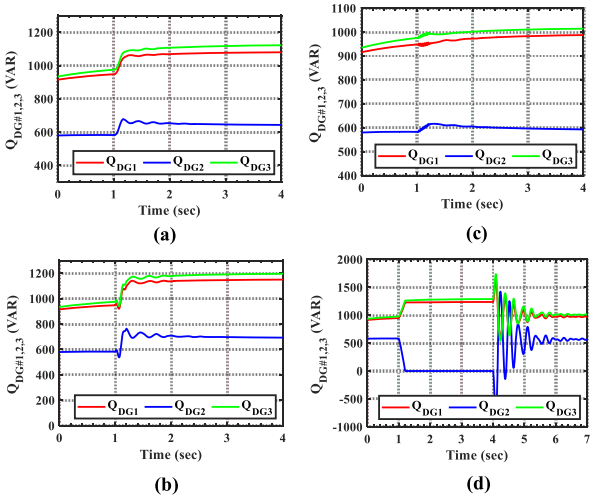

Fig. 10. Dynamic response of AC-MG for various senarios: Reactive power of DGs (a) increasing load, (b) imbalance load, (c) nonlinear load, (d) plug&play of DG2

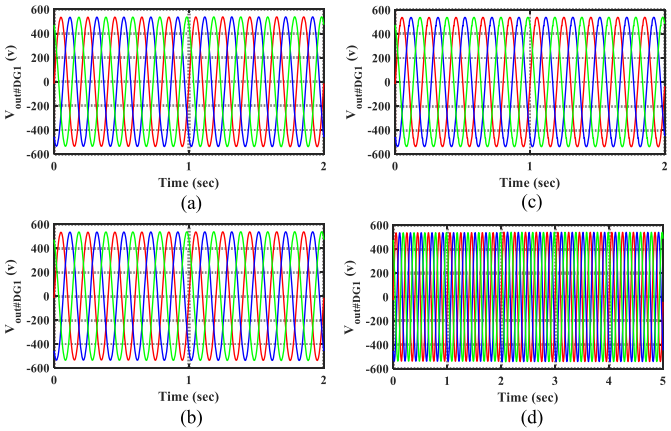

Fig. 11. The output voltage of DG1 unit under various senarios: (a) increasing load, (b) imbalance load, (c) nonlinear load, (d) plug&play of DG2.

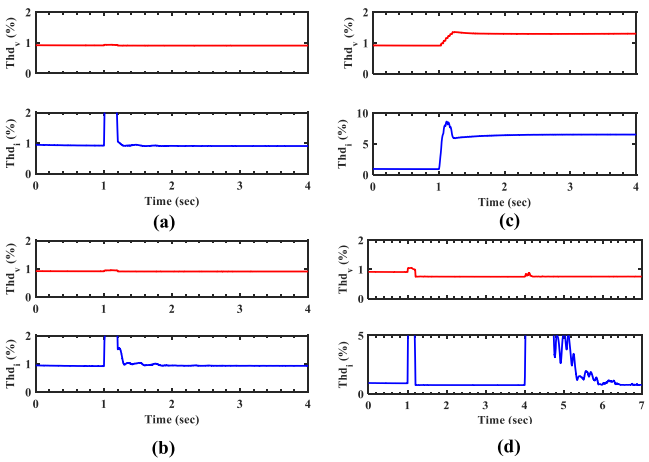

Fig. 12. The total harmonic distoration of the output voltage and the output current during various senarios: (a) increasing load, (b) imbalance load, (c) nonlinear load, (d) plug&play of DG2

At first, a sudden three-phase inductive load with power 0.05 p.u is applied at the terminal of DG3 at $t = 1s$. Then, a single-phase load with 0.8 p.u of power and 0.85 of power factor is applied to phase A of the local load of DG2. In continue, a three-phase six-pulse diode-bridge rectifier is connected in parallel to the local load of DG1 with 0.7 p.u of power to emulate nonlinear loading scenario. Finally, it is assumed that DG2 is disconnected from the MG at t = 1 s, and then, is connected at t = 4 s. Figs. 9 and 10 show MG active and reactive power sharing during the all scenarios. It is clear that the proposed control technique can sufficiently share the active and reactive power between the DGs. Fig. 11 shows the instantaneous voltage at the terminal of DG1 unit. As can be observed, the designed controller maintains the voltage in enduring regulating mode, and the reference is tracked with an error between 2-3%. Fig. 12 illustrates the total harmonic distortion (THD) of the output current and voltage of DG units. As shown, the THD percent of terminal voltage is maintained constant at 1% under all loading conditions, whereas the worst case of THD of the output current of DGs is about 10% when the nonlinear load is applied. The obtained results in this section validate the proposed control strategy.

VI. Conclusion

In this study, an intelligent PR controller was applied in inner loop of primary control level to adjust the DG's interfacing converter. Compared to previous studies, the main contribution of this scheme is that the the PR coefficients are regulated without prior knowledge of the MG dynamics. The proposed controller's key features are the minimal computational intricacy, online learning ability, and no requirement for prior knowledge of MG dynamics. The approach's effectiveness was illustrated on VSC-based DGs in an islanded AC-MG. Minimizing the THD and correcting power-sharing were the main objectives behind the BEL-based PR method. A stability analysis was also conducted to examine the stability of dominant frequency modes of the whole AC-MG using the proposed control scheme. Finally, the simulation results obtained from a benchmark AC-MG demonstrated the effectiveness of the proposed solution with different operational conditions.

VII. Acknowledgment

This work was supported by the Reliable Power Electronic-Based Power System (REPEPS) project at the AAU Energy, Aalborg University as part of the Villum Investigator Program funded by the Villum Foundation.

References

[1] S. Parhizi, H. Lotfi, A. Khodaei and S. Bahramirad, "State of the Art in Research on Microgrids: A Review," IEEE Access, vol. 3, pp. 890–h925, 2015, doi: 10.1109/ACCESS.2015.2443119.

[2] A. A. Derbas, M. Kheradmandi, M. Hamzeh and N. D. Hatziargyriou, ""A Hybrid Power Sharing Control to Enhance the Small Signal Stability in DC Microgrids," IEEE Transactions on Smart Grid, vol. 13, no. 3, pp. 1826-1837, May 2022, doi: 10.1109/TSG.2022.3156850.

[3] R. Heydari et al., "Robust High-Rate Secondary Control of Microgrids With Mitigation of Communication Impairments," IEEE Transactions on Power Electronics, vol. 35, no. 11, pp. 12486–12496, Nov. 2020, doi: 10.1109/TPEL.2020.2986368.

[4] A. A. Derbas and M. Hamzeh., "A New Power Sharing Method for Improving Power Management in DC Microgrid with Power Electronic Interfaced Distributed Generations,"2019 27th Iranian Conference on Electrical Engineering (ICEE), 2019, pp. 624-629, doi: 10.1109/IranianCEE.2019.8786470.

[5] J. M. Guerrero, J. C. Vasquez, J. Matas, L. G. De Vicu˜na, and M. Castilla, "Hierarchical control of droop-controlled ac and dc microgridsˆaa general approach toward standardization," IEEE Transactions on industrial electronics, vol. 58, no. 1, pp. 158–172, 2010.

[6] O. Palizban and K. Kauhaniemi, "Hierarchical control structure in microgrids with distributed generation: Island and grid-connected mode," Renewable and Sustainable Energy Reviews, vol. 44, pp. 797–813, 2015.

[7] M. Ghazzali, M. Haloua, and F. Giri, "Modeling and adaptive control and power sharing in islanded ac microgrids," International Journal of Control, Automation and Systems, vol. 18, no. 5, pp. 1229–1241, 2020.

[8] A. Vijay and S. Doolla, "Performance of droop control techniques under nonlinear loading conditions: Uniform and nonuniform configurations," IEEE Systems Journal, vol. 15, no. 2, pp. 2245–2256, 2020.

[9] H. Bevrani and S. Shokoohi, "An intelligent droop control for simultaneous voltage and frequency regulation in islanded microgrids," IEEE transactions on smart grid, vol. 4, no. 3, pp. 1505–1513, 2013.

[10] B. Lin et al., "Selective Pole Placement and Cancellation for Proportional–Resonant Control Design Used in Voltage Source Inverter " IEEE Transactions on Power Electronics, vol. 37, no. 8, pp. 8921–8934, February 2022.

[11] B. Li, W. Yao, L. Hang and L. M. Tolbert, "Robust proportional resonant regulator for grid-connected voltage source inverter (VSI) using direct pole placement design method," IET Power Electronics, vol. 5, no. 8, pp. 1367–1373, September 2012.

[12] A. Vidal et al., "Assessment and Optimization of the Transient Response of Proportional-Resonant Current Controllers for Distributed Power Generation Systems," IEEE Transactions on Industrial Electronics, vol. 60, no. 4, pp. 136–1383, April 2013.

[13] B. Amini, R. Roshanfekr, A. Hajipoor, S. Mousavi,, "Interface converter control of distributed generation in microgrids using fractional proportional-Resonant controller," Electric Power Systems Research, vol. 194, pp. 107097, issn. 0378–7796, 2021, doi:10.1016/j.epsr.2021.107097.

[14] M. Qutubuddin and N. Yadaiah, "Modeling and implementation of brain emotional controller for permanent magnet synchronous motor drive," Engineering Applications of Artificial Intelligence, vol. 60, pp. 193–203, 2017.

[15] R. Khezri et al., "Intelligent coordinators for automatic voltage regulator and power system stabiliser in a multi-machine power system," IET Generation, Transmission & Distribution, vol. 14, no. 23, pp. 5480–5490, 2020, doi: 10.1049/iet-gtd.2020.0504.